Nanoscale

Accepted Manuscript

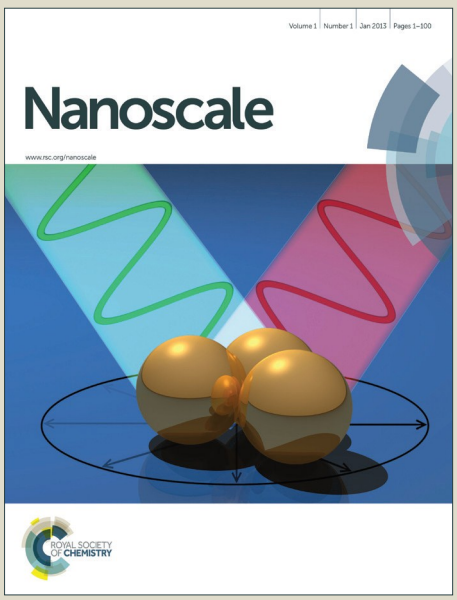

ROYAL SOCIETY OF CHEMISTRY

www.rsc.org/nanoscale

Journal Name

ARTICLE

Carboxylated Nanodiamonds Inhibit γ-Irradiation Damage of Human Red Blood Cells

Received 00th January 20xx,
Accepted 00th January 20xx

DOI: 10.1039/x0xx00000x

www.rsc.org/

K. Santacruz-Gomez*[a,b], E. Silva-Campa[c], R. Melendrez-Amavizca[c], F. Teran Arce[b,d,g], V. Mata-Haro[e], P. B. Landon[b,d], C. Zhang[f], M. Pedroza-Montero[c] and R. Lal*[b,d]

Nanodiamond when carboxylated (cND) acts as a reducing agent and hence could limit oxidative damage in biological systems. Gamma (γ)-irradiation of whole blood or their components is required in immunocompetent patients to prevent transfusion-associated graft versus host disease (TA-GVHD). However, γ-irradiation of blood also deoxygenates red blood cells (RBCs) and induces oxidative damage, including abnormalities in cellular membranes and hemolysis. Using atomic force microscopy (AFM) and Raman spectroscopy, we examined the effect of cND on γ-irradiation mediated deoxygenation and morphological damage of RBCs. γ-radiation induced several morphological phenotypes, including stomatocyte, codocyte and echinocyte. While stomatocytes and codocytes are reversibly damaged RBCs, echinocytes are irreversibly damaged. AFM images show significantly fewer echinocytes among cND-treated γ-irradiated RBCs. Raman spectra of γ-irradiated RBCs had more oxygenated hemoglobin patterns when cND-treated, resembling those of normal, non-irradiated RBCs, compared to the non-cND-treated RBCs. cND inhibited hemoglobin deoxygenation and morphological damages, possibly by neutralizing free radicals generated during γ-irradiation. Thus cNDs have therapeutic potential to preserve the quality of stored blood following γ-irradiation.

Introduction

Irradiation of red blood cells (RBCs) with gamma (γ) rays is commonly used to inactivate T-lymphocytes and thus prevent transfusion-associated graft versus host disease (TA-GVHD) in immunocompromised patients.[1] Gamma irradiation is applied to whole blood, as well as blood components. However, direct application to whole blood reduces pathogens and inactivates lymphocytes in a single step, thus allowing the use of the sterilized product as whole blood or their single components separately.[2] Blood γ-irradiation at a dose of 25 Gy inhibits lymphocyte proliferation[3] by targeting their DNA, while the other blood cells remain viable.[4] Radiation energy-induced damage in DNA is called the direct action of radiation[5] and is the primary cause of cytotoxicity during radio-therapies.[6] However direct action of irradiation is not the only concern during radiotherapies.[7] Deleterious effects on RBCs have also been reported following γ-irradiation of blood,[8] and which deteriorate further during storage.[9] For this reason, the shelf life of blood and blood components is reduced after irradiation. [10] These effects are due to the indirect action of radiation (radiolysis) in cells.[11] Radiolysis of water molecules generates reactive oxygen species (ROS), including hydroxyl radicals (•OH) and hydrogen peroxide (H_2O_2).[12] High concentrations of ROS induce oxidative damage and subsequent cytotoxicity,[13] including rearrangement of cytoskeletal proteins,[14] membrane damage[15] and subsequent hemolysis.[16, 17] Therefore, antioxidant strategies are still needed in order to prevent the deleterious effect of ionizing radiation. [18, 19] Nanodiamond (ND) is a promising material for biological applications due to its biocompatibility.[20] However, ND biocompatibility varies as a function of its cellular uptake, as well as its physicochemical properties, including size, shape and surface charge.[21, 22] NDs can be easily functionalized by chemical methods,[23] allowing NDs deagglomeration[24] and providing a suitable multi-functional platform.[25] In particular, carboxylated nanodiamonds (cNDs) have a relatively strong negative surface charge in physiological solutions, thus providing good colloidal stability,[26, 27] and allowing electrostatic coupling of positively-charged biomolecules for therapeutic applications.[28] Significantly, cND has been reported to have high cellular uptake[29] as well as limited cytotoxicity at low concentrations.[30] Here, we have examined the effect of cNDs on the morphology and oxygenation states of RBCs irradiated *in vitro* with a Cobalt-60 γ-ray source. Using AFM imaging, we obtained

[a] Departamento de Física. Universidad de Sonora. Blvd. Luis Encinas y Rosales s/n. C.P. 83000. Hermosillo, Sonora, México
[b] Department of Mechanical and Aerospace Engineering, University of California, San Diego, 9500 Gilman Drive, La Jolla, USA.
[c] Departamento de Investigación en Física. Universidad de Sonora. Hermosillo, Sonora, México
[d] Department of Bioengineering, University of California San Diego, La Jolla, CA.
[e] Centro de Investigación en Alimentación y Desarrollo, AC. Carretera a la Victoria Km 0.6. Hermosillo, Sonora, México.
[f] Department of Nanoengineering, University of California, San Diego.
[g] Currently at Division of Translational and Regenerative Medicine, Department of Medicine, University of Arizona, Tucson, AZ, USA.

Electronic Supplementary Information (ESI) available. See DOI: 10.1039/x0xx00000x

morphometric features of RBCs upon exposure to 20, 40 and 60 Gy dosages of gamma irradiation. AFM images reveal pathological morphologies of RBCs associated with abnormal distributions of hemoglobin (Hb) following γ-irradiation. Among these three main RBC phenotypes, stomatocytes predominate in cND-treated RBCs, whereas echinocytes, a prelytic phase, are predominant in RBCs without cNDs. Raman spectroscopy data suggest that cNDs reduce Hb deoxygenation in irradiated RBCs. These findings indicate that γ-radiation damage in RBCs is reduced by the presence of cNDs. Thus cNDs have therapeutic potential to preserve the quality of stored blood following γ-irradiation.

Experimental

Carboxylation of detonation nanodiamond (DND). Stock aqueous suspensions of (grade G01) DNDs (4 % by weight) were purchased from PlasmaChem (D-12489 Berlin). Their surface was functionalized with carboxyl groups using a strong acid treatment, as follows.[42] In a round bottom flask with 30 ml of a 9:1 H_2SO_4:HNO_3 mixture, 1 ml of DNDs (stock solution) was added and left stirring for 72 hours at room temperature. Immediately upon adding 50 ml of 0.1 M aqueous NaOH, the flask was placed in an oil bath at 90 ºC and left stirring for 2 hours. 20 ml of 0.1 M aqueous HCl were added and the mixture was left stirring at 90 °C for 2 additional hours. The DNDs reaction mixture was then immediately washed (by centrifugation at 20076 g for 5 minutes and decanting) with 15 mL of deionized water several times. After centrifugation, the sediment was dispersed in distilled water and dried in a vacuum oven at 45 ºC. The dried cND powder was suspended in water (0.04 and 0.004 % by weight), bath-sonicated for 15 minutes and vigorously shaken. This was followed by probe ultrasonication in an ice bath for 5 minutes in 30 seconds cycles. Particle sizes of DNDs and cNDs were determined by dynamic light scattering (DLS) using a Zetasizer Nano ZSP (Malvern). Characterization by transmission electron microscopy (TEM) was carried out with a Hitachi H8100 (200 kV). ND cytotoxicity depends on ND size and surface chemistry. Non-toxic effects on RBCs were reported for cNDs with sizes of ~ 100 nm with concentrations of 0.02, 0.05 and 0.005 mg/mL.[1, 31] Also, NDs used as therapeutic agents were non-cytotoxic to other cell lines.[32] Therefore, 0.04 mg/ml lies within the cND concentration considered to be safe.

Sample preparation and irradiation. Whole blood was collected by phlebotomy from healthy donors, in vacuum tubes containing ethylene diamine tetra-acetic acid (EDTA) anticoagulant solution. Whole blood was incubated with cND to a final concentration of 0.04 mg/mL during 2 hours at 4 °C and constant shaking. Two groups of vacuum tubes, one group containing blood treated with cNDs and another with blood only, were exposed to gamma radiation at dosages of 0, 20, 40 and 60 Gy. Two tubes, one of each group, were placed together in the Gammacell for each dose, and irradiated using a Cobalt-60 (Co60) gamma-ray source at 20, 40 and 60 Gy with a MS Nordion Gammacell 220 Excel, at a dose rate of 0.8 Gy/s. The irradiation chamber is a closed, thin-walled, non-corrosive metal cylinder with a lift-out full width door. The chamber is 15.49 cm in diameter and 20.47 cm in height, with a volume of 3.7 L. The access port is 20.09 cm high and 15.24 cm wide. The blood samples were placed in the center of the cylindrical irradiation chamber and, in the position of irradiation, the distance between the Co-60 gamma sources and the blood samples was around 13 cm. The sealed gamma sources, in form of 14 pencils, are homogeneously distributed around the irradiation chamber. Immediately after irradiation, RBCs were separated from whole blood by centrifugation at 800g for 5 min at 4 °C. The supernatant containing the plasma was discarded (and collected for the hemolysis test at 4 °C) and the packed RBCs were washed three times with sterile phosphate buffered saline solution (PBS) 10× and centrifuged at 500g for 2 minutes at 4 °C. RBCs were diluted to a final concentration of 0.5% of cells in sterile PBS (pH 7.4). All the experiments using human blood were approved by The Ethical Human Subject Research Committee. Formal written consent was obtained from the subjects prior to blood collection.

AFM Images. Topographic images of nanodiamonds were obtained in peak force tapping using a Multimode AFM from Bruker (Santa Barbara, CA) equipped with a Nanoscope V controller and run by a Nanoscope version 9.1 software (also from Bruker). AFM cantilevers (ppp-nchr type, from Nanosensors) with nominal spring constants of 42 N/m were used. Images of RBCs were obtained in contact mode using an XE-Bio AFM from Park Systems. Microfabricated Aluminum coated cantilevers (PPP-CONTSCR type from Nanosensors) with a spring constant of 0.01 N/m were used. Images were obtained in air for all samples.

Optical Microscopy. Fluorescence and bright field images of cNDs interacting with RBCs were obtained using an inverted optical microscope (Olympus, 1X71) equipped with a Hamamatsu CCD camera. cNDs were excited with a wavelength of 482±17 nm and the emitted light was collected in the 536±20 nm range.

Raman Microspectroscopy measurements. 200 µl of the RBC:PBS suspension were diluted in 1 mL of PBS and deposited on a silicon substrate coated with poly-l-lysine (0.01% sterile-filtered, P 4707 Sigma-Aldrich) to reduce background noise in Raman spectra. The spectra were collected using a LabRAM Raman Micro-spectrometer (Horiba Jobin Yvon) with a 632 nm excitation wavelength laser. Spectra in the range of 600-1700 cm-1 of 30 single RBCs were obtained and averaged for each sample. The data were processed and analyzed using Origin software (Origin Pro 9.0).

Hemolysis of RBCs. The percentage of hemolysis was determined from the free Hb released in blood plasma by RBCs. The plasma (supernatant) was carefully collected from whole blood (centrifugation at 2200×g for 5 min at 4 °C), after γ –irradiation at 0, 20, 40 and 60 Gy doses during 24, 48 and 72 hours. The absorbance was read from 350 to 600 nm using a microplate Spectrophotometer (xMark, BioRad). The concentration of free Hb was quantified applying the Harboe method[33] with polychromatic analysis (hemoglobin (mg/L) = 1.65 mA415 - 0.93 mA380 - 0.73 mA470). 50 µL of whole blood were diluted in deionized water (1:10). To collect the released Hb, blood was centrifuged at 2200×g for 5 min at 4 °C. When the free hemoglobin was obtained, the % of hemolysis was determined as follows: % Hemolysis = [(100-Hematocrit) X Hb free in plasma or suspending medium]/Total Hb. The hematocrit is used to correct the error of overestimation of the percentage of hemolysis in relation to the volume of the fluid.[34]

Viability. The number of RBCs viable in presence of cNDs was estimated using the blue trypan dye exclusion test. 30 µl of a RBC treated with cNDs suspension were added into 30 µl of 0.4% Trypan Blue solution and mixed thoroughly. Dead cells (blue stained) and viable cells (unstained) were counted using a hemocytometer. The percentage of viable cells was calculated as follows:

Cell Viability (%) = total viable cells (unstained) ÷ total cells (stained and unstained) × 100.

Results and discussion

The DNDs used in our work owe their name to the original explosion procedure used to fabricate them.[35] Prior to their use with RBCs, DNDs were disaggregated following the carboxylation protocol described in the experimental section. While stock DNDs had a mean diameter of ~300 nm (Figure 1A), the diameter of cNDs was decreased to ~37 nm (Figure 1B). At the same time, the zeta potential decreased from -24.2 mV (for DNDs) to -48.6 mV (for cNDs). ND clusters are typical in DND, consisting of small NDs (~4-20 nm) core by a combination of graphitic shell, soot structures and graphitic ribbon-like structures.[36]

AFM measurements of the stock DND sample also revealed the presence of ND particles aggregated into larger clusters (Fig. 1C). Their heights ranged from 10 to 500 nm and had overdispersed distributions with a mean value of 61 nm and standard deviation of 93 nm. Streaks were frequently observed in scan lines (both in regular tapping and peak force tapping), suggesting that weakly bound particles were dislodged from the clusters by the AFM tip. DND disaggregation following carboxylation was confirmed in the AFM images (Fig. 1D and 1E). Height histograms (not shown) showed the presence of two ND populations, one with a peak around 25 nm and another at 130 nm. Images with higher magnification displayed the presence of cubic crystallite structures. However, we could not observe any substructure on these crystallites.

Using optical microscopy we verified cND uptake by RBCs. Figure 2 shows individual RBCs without cNDs (Figure 2A) and RBCs incubated with cNDs for 2 hours (Figure 2B). As we could not detect cellular cND uptake, cNDs are likely to be localized outside the RBCs (Figure 2B inset). However, the proximity of cNDs to RBCs, observed by bright field (Figure 2C) and fluorescence optical microscopy (Figure 2D), suggests a potential interaction of cNDs with RBCs membranes as reported for cNDs with ~100 nm sizes. [31] Figure 2C and Figure 2D show RBCs after 2 hours of incubation with cNDs.[37]

Results of the effect of cNDs on RBCs-oxidative damage induced by γ-irradiation are presented in figure 3. AFM images of non-irradiated RBCs (with and without cNDs) displayed a fairly homogeneous morphology and size distribution (Figure 3A). Following γ-irradiation at dosages of 40 Gy or higher, RBCs (cND-treated and untreated) had modified morphologies and heterogeneous size distributions (Figure 3 B and C).

Although normal RBC morphology was altered for all γ-irradiated samples, the original RBC morphology was better preserved for γ-irradiated RBCs when treated with cNDs (Figure 3C).

Populations of morphologically abnormal RBC subtypes, i.e. stomatocytes, codocytes and echinocytes, were identified *in vitro* upon γ-irradiation (A brief description of the RBCs shape abnormalities and their features is given in Supporting Information, Figure S1). Abnormal morphologies of RBCs are associated with pathological processes,[38] but they can also result in response to chemical or physical stimuli[39-41] significantly deformed RBC subtypes were evident for all samples irradiated at 60 Gy. Echinocytes (level 3, prelytic phase), characterized by the presence of spicules on the membrane (Figure 3B and E), were observed only for cND- untreated RBCs at dosages higher than 40 Gy. In addition, lower level echinocytes, characterized by alterations in the central pallor (Figure S1 A and C), were also observed at these irradiation dosages. A different alteration of RBC morphology following γ-irradiation, stomatocytes, was detected by AFM only in samples treated with cNDs (Figure 3C and F). Stomatocytes did not show vesiculation and the central pallor remained (Figure S1, C Supporting Information).

Stomatocytes have reversible deformations, recovering their normal RBC morphology after a stress is lifted, whereas the morphological transformation for echinocytes is irreversible, and followed by cell death. Using AFM we analyzed the different morphologies of cND-treated and non-treated RBCs at four radiation doses (Figure S2, Supporting Information). Populations of N=50 cells were analyzed for each treatment and dose (total population of 400 cells). Although the percentage of abnormal RBCs increased (consequently decreasing the percentage of normal RBCs) with γ-irradiation dose both for cND-treated and non-treated samples, the effects were more pronounced for RBCs without cNDs, particularly at the higher doses.

The distribution and molecular configuration of hemoglobin (Hb) influence the biconcave shape and deformability of RBCs.[42] Thus, in order to understand the influence of cNDs on RBCs integrity, we investigated the oxygenation states of γ-irradiated RBCs (cNDs-treated and non-treated) using Raman spectroscopy. We first verified that cNDs did not appear to have negative effects on the oxygenation state of RBC (Figure 3G) as described previously.[31]

Journal Name

ARTICLE

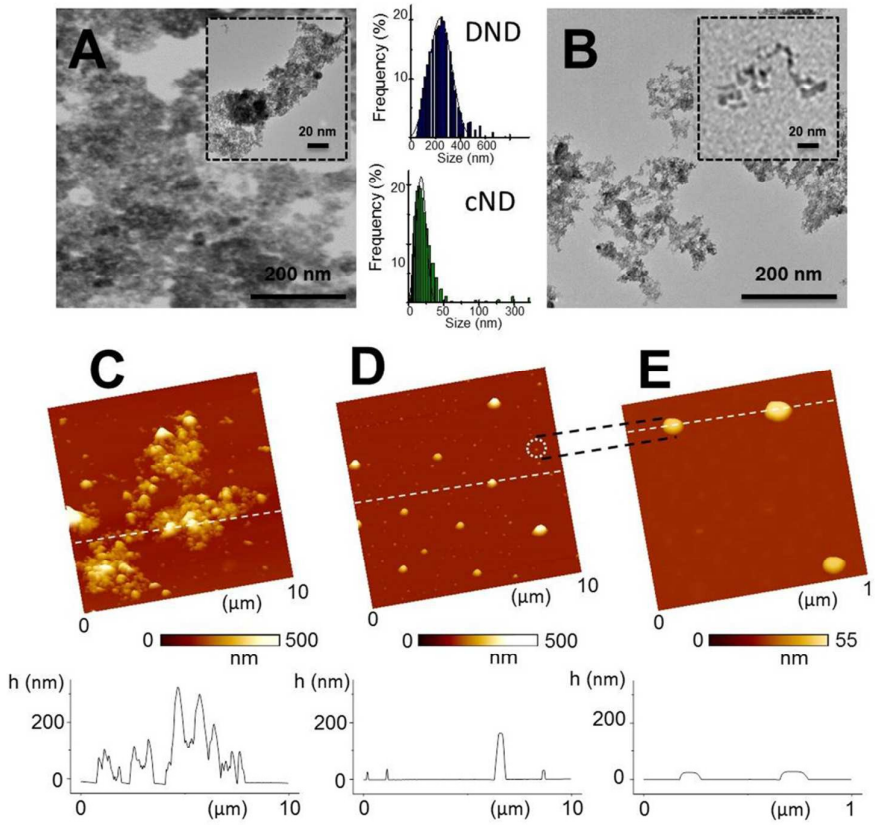

Fig. 1 (A) TEM images of as-received commercial DNDs (left) and their size distribution measured by DLS (up). (B) TEM images of cNDs and their size distribution measured by DLS (bottom). (C)-(E) AFM images of (C) DND clusters and (D)-(E) carboxylated NDs. Two populations of cNDs are observed in the cross section (D). Higher magnification images display more clearly the morphology of the ND particles (E). The presence of cubic crystallites was suggested in some images.

The RBCs oxygenation state was evaluated at oxy-Hb and deoxy-Hb Raman peaks. Average spectra of irradiated and non-irradiated samples showed a number of peaks observed for oxygenated and deoxygenated hemoglobin after 20, 40 and 60 Gy of γ-irradiation. Although, additional semi-deoxygenated patterns were observed for samples irradiated at 60 Gy with and without cNDs (Figure 3 G), the mitigating effects of cND became apparent when stomatocytes and echinocytes were analyzed separately (Fig. 3H and 3I). To investigate the relationship between oxygenation states and cell morphology, we subsequently separated the analysis of Raman spectra for different RBC subtypes: echinonocytes (only observed in absence of cNDs) and stomatocytes (only observed in presence of cNDs). The peak location and intensity of the Raman spectra of stomatocytes, echinocytes and normal RBCs were distinctly different at 60 Gy. The spectra of normal RBCs contained a well-defined intensity peak located at 1224 cm^{-1} (Figure 3H). This peak is associated with the C-H methane in plane bending vibration typical of the oxygenated hemoglobin (oxy-Hb) state.[43] The transition to a deoxygenated hemoglobin state (deoxy-Hb) could be observed by a change in the intensity of this peak, and the appearance of a new band at 1212 cm^{-1}. Significantly, stomatocytes and codocytes (spectra not showed) are partially deoxygenated while echinocytes are severely deoxygenated. This is further supported by analyzing the Raman spectra in the 1500-1700 cm^{-1} region (Figure 3I). Bands

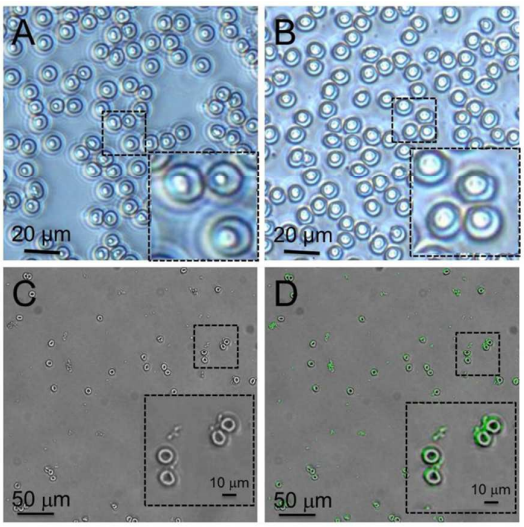

Fig. 2 Optical microscopy (bright field) images of single RBCs obtained (A) in absence of cNDs and (B) in presence of cNDs. The insets in (A) and (B) show, with greater detail, single cells in the regions marked with dashed squares. (C) Bright field optical images of RBCs suspended in PBS and treated with cNDs using a 10x objective. (D) Fluorescence image superimposed on the bright field image (C). The inset shows cNDs in the proximity of RBCs. cNDs were excited at 482±17 nm and the emitted light was collected in the 536±20 nm range (shown in green).

related with oxy-Hb states (1565, 1588 and 1620 cm^{-1}) were identified in normal RBC samples. Only the peak located at 1620 cm^{-1} was observed for stomatocytes and echinocytes, with some intensity variations. Whereas, deoxy-Hb associated bands, including 1546 cm^{-1} and 1606 cm^{-1}, were notoriously present in echinocytes. Comparing the Raman spectra of normal RBCs shape and abnormal subtypes (echinocytes and stomatocytes) allow us to confirm cellular deoxygenation after γ-irradiation related to the presence or absence of cND respectively.

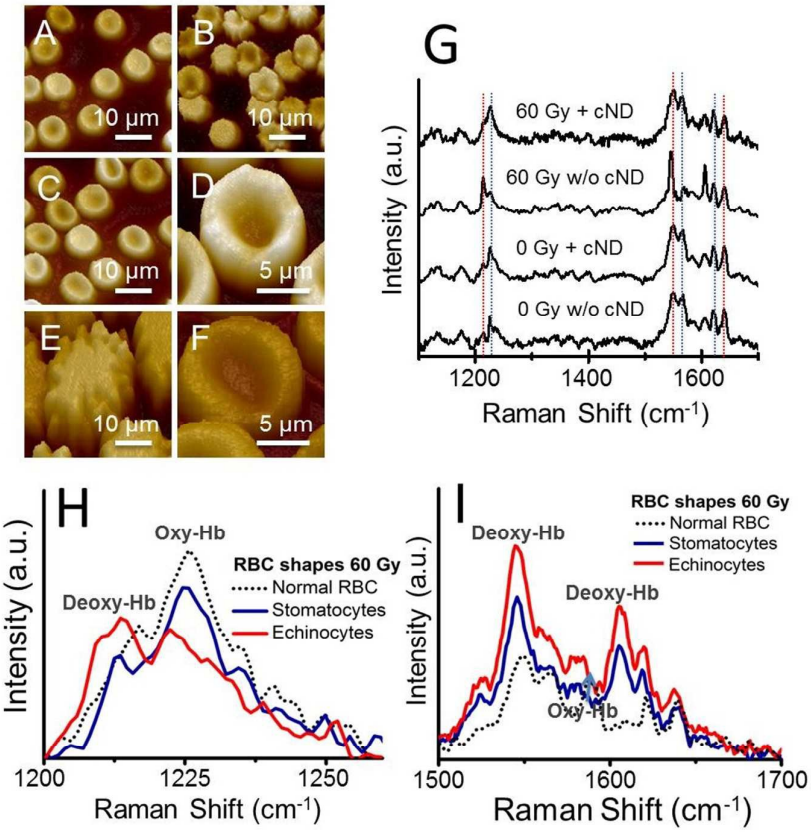

Fig. 3 (A) Non-irradiated RBCs, not treated with cNDs, (control) showing a homogeneous distribution, in shape and size. (B) RBCs without cNDs after 60 Gy of γ-irradiation. (C) RBCs treated with cNDs following 60 Gy of γ-irradiation. (D) Normal RBC morphology, of ~10 µm size with a central pallor of ~3 µm. (E) Echinocytes observed in non cND-treated samples, characterized by convex rounded spicules. (F) Stomatocytes observed in cND-treated samples, exhibit bi-concave, disk shaped morphologies. (G) Two lower spectra: Raman spectra of non-irradiated RBC controls (RBCs with and without cND) indicating that cNDs do not affect oxygenation states of Hb. Two upper spectra: Raman spectra of samples irradiated with 60 Gy γ-irradiation, with and without cNDs. RBCs in presence of cNDs appear more oxygenated after 60 Gy of γ-irradiation compared with samples without cND treatment. Red and blue dotted lines indicate deoxy-Hb and Oxy-Hb peaks respectively. Comparison between Raman spectra of a normal RBC (black dotted lines) and abnormal RBC subtypes in two regions: (H) 1200-1250 cm^{-1} and (I) 1500-1700 cm^{-1} after 60 Gy of γ-irradiation. Spectra of stomatocytes are shown in blue lines and of echinocytes in red lines.

Journal Name

ARTICLE

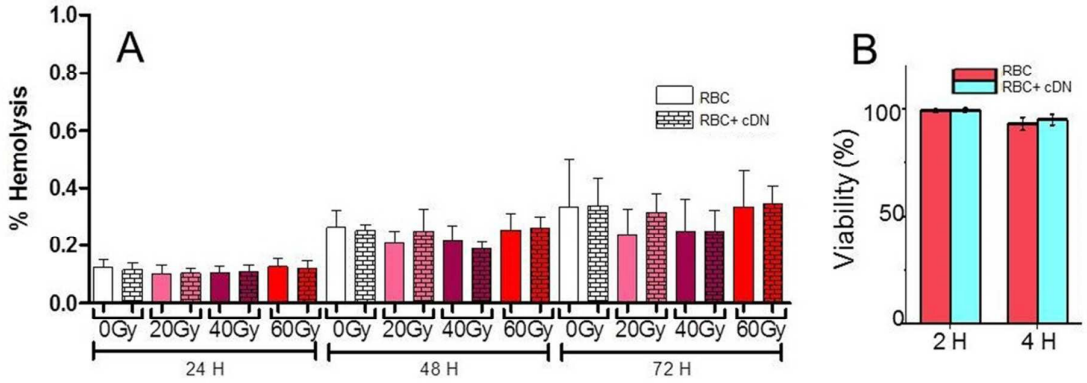

Fig. 4 (A) Relative hemolysis of γ-irradiated RBCs in presence and absence of cNDs at different radiation dosages after 24, 48 and 72 hours treatment. (B) Percentages of viable non-irradiated RBCs (cND-treated and untreated) by the blue trypan assay after 2 and 4 hours of incubation.

Oxy-Hb appears due to the low spin of iron (S=1/2) which can bind oxygen showing a relaxed conformation, the R state.[27] On the other hand, deoxy-Hb appears due to the high spin of iron (S=2), the T-state.[44] Hb deoxygenation can be observed in the peaks located at 1213 cm^{-1}, 1545 cm^{-1} and 1606 cm^{-1}. The difference between Raman peaks corresponding to normal and abnormal RBC subtypes allows us to confirm cellular deoxygenation, total or partial, induced by γ-irradiation.

ROS are responsible for Hb oxidation and denaturalization of structural proteins, as well as for oxidative hemolysis.[45] We found no significant hemolysis difference between populations of cND-treated and untreated RBCs stored for 1-3 days (Fig. 4A). The observed values of hemolysis were within the normal levels of blood banking guidelines.[34] These data show that: i) cND-treatment does not induce hemolysis, and ii) gamma irradiation does not induce early hemolysis in doses below 60 Gy. Nevertheless, hemolysis will potentially become significant late in storage, as described elsewhere.[46, 47] Furthermore, the morphological damage reported here (Figure 3A-F) demonstrates that for doses higher or equal to 20 Gy, gamma irradiation has a significant impact on *in vitro* quality of RBCs. To elucidate if these effects were influenced by the presence of cNDs, RBC viability was studied by the trypan blue exclusion assay. No significant cytotoxic effects were observed on RBCs with and without cNDs after 2 and 8 hours (Figure 4B).

Exposure of RBCs to ionizing radiation leads to biological damage by ionization of atomic and molecular species. Because of its high content in the cytoplasm and ionization energy (~10 eV)[48] well below the energies of the γ-radiation emitted by Cobalt-60 (~ MeV),[49] water is the most probable molecule to be ionized .[50] As a result, the water molecule is dissociated into free radicals, including hydrogen ions (H^+) and hydroxyl (OH·) radicals. [51]

Free radicals are chemically reactive, and recombine quickly to produce reactive oxygen species (ROS), including hydroperoxyl (HO_2^-) and peroxide (H_2O_2) (Figure S4, Supporting Information). Some of these species neutralize each other while others spread throughout the cytoplasm to reach distant molecules causing oxidative damage. Further, the Fe^{2+} ions in Hb can be oxidized into Fe^{3+} (which cannot bind oxygen), when interacting with HO_2^-, OH· or H_2O_2 [40] (Equation 1), resulting in RBCs deoxygenation.

$$HO_2\cdot + Fe^{2+} \rightarrow HO_2^- + Fe^{3+}$$

$$OH\cdot + Fe^{2+} \rightarrow HO^- + Fe^{3+}$$

$$H_2O_2 + Fe^{2+} \rightarrow HO + Fe^{3+} + HO^- \quad (1)$$

Oxidative damage is believed to be directly proportional to the concentration of radiation generated ROS minus the neutralized ROS.[52] Although we did not measure the concentration of ROS, based on our data we hypothesize that the concentration of ROS decreases for cND-treated RBCs due to an increase in the concentration of neutralizing species (Supplementary Information, Figure S5), possibly due to the presence of COO- radicals on the cND surface. Earlier work reported nanodiamonds-mediated radioprotective effects by the neutralization of free radicals.[53] According to this scenario, cNDs reduce RBC deoxygenation by decreasing: i) oxyHb (Fe^{2+}) oxidation into methemoglobin (Fe^{3+}) a Hb form which cannot bind oxygen,[54] and ii) membrane damage of RBCs by avoiding the oxidation of structural proteins responsible of echinocytes transformation.

Here, it is worth considering the potential effect of γ-irradiation on lymphocytes. Inactivation of lymphocytes is due to the direct effect[55] of ionizing radiation (i.e. ionization of DNA and other biomolecules inside the cell's nucleus), induced cell cycle arrest (inactivation),[56] and apoptosis.[57] Although in this work we describe indirect effects of ionizing radiation on

RBCs (morphological damage, Hb deoxygenation and hemolysis) and protection from indirect radiolysis, we hypothesize that lymphocytes are going to be inactivated at doses above 25 Gy, as in the usual γ-irradiation protocol. However, the overall blood product quality would be improved by reducing storage damage.

While the parameters for the appropriate use and maintenance of blood are established,[58, 59] the biochemical impact that storage has on its components is still under discussion.[16] A major concern about blood transfusion is the potentially enhanced oxidative damage produced on its irradiated components. [60-62] Blood banking authorities and publications on the subject suggest that irradiated blood and blood components should be transfused as freshly as possible in order to decrease the unexpected adverse effects on patients.[17] Although blood irradiation is currently the only method available to prevent TA-GVHD,[1] freshly irradiated units are not always readily accessible. In this case, the preservation of the irradiated products remains a critical issue. In this work, the reduction of RBCs deoxygenation and morphological damage after γ-irradiation were demonstrated in presence of cNDs. Our data suggests that cNDs enhance RBC recovery immediately after irradiation, potentially contributing to their preservation during storage, as reported recently by our group.[63] Minimization of the side effect of gamma irradiation on RBCs following irradiation improves the quality of blood for transfusion. These results suggest that cNDs maintain the shape of RBCs, without leading to irreversible morphologies, e.g. echinocytes, and maintain more oxygenated patterns which contribute to accelerating the recovery of RBCs *in vitro*, as well as potentially *in vivo*, on patients. Nevertheless, *in vivo* assays are necessary to substantiate the potential application of this technique in blood banks.

Conclusions

In summary, we significantly disaggregated DNDs and improved their colloidal stability in water by surface carboxylation, resulting in the cNDs used in our experiments. Gamma irradiation induced three RBCs morphological phenotyic subtypes, including codocytes, echinocytes and stomatocytes in a dose dependent manner. Echinocytes appeared in cND-untreated samples, exhibiting deoxy-Hb states. Stomatocytes were observed in samples treated with cNDs and appeared to be more oxygenated than echinocytes. These *in vitro* results suggest that cND inhibits radio-induced Hb deoxygenation and reduces the associated morphological damage. The presence of damaged RBCs, e.g. echinocytes, has clinical significance.[64] Firstly echinocytes present in a blood bag are transfused into the patient, and secondly echinocytes represent irreversible morphological damaged RBCs and cellular death,[65] resulting in the depletion of the RBC concentration in blood. Thus cNDs have therapeutic potential to preserve the quality of stored blood following γ-irradiation.

Acknowledgements

This work was supported by the Universidad de Sonora. K. Santacruz-Gomez thanks a Post-doctoral Fellowship (237085) provided by Consejo Nacional de Ciencia y Tecnología (CONACyT) during 2015-2016.

References

1. J. Chapman, R. Finney, K. Forman, P. Kelsey, S. Knowles, J. Napier, P. Phillips, R. Mitchell, M. Murphy and A. Waters, *Transfus Med*, 1996, **6**, 261-271.
2. L. D. Fast, M. Nevola, J. Tavares, H. L. Reddy, R. P. Goodrich and S. Marschner, *Transfusion*, 2013, **53**, 373-381.
3. E. Góes, J. Borges, D. Covas, M. Orellana, P. Palma, F. Morais and C. Pelá, *Transfusion*, 2006, **46**, 34-40.
4. L. Button, W. DeWolf, P. Newburger, M. Jacobson and S. Kevy, *Transfusion*, 1981, **21**, 419-426.
5. D. t. Goodhead, *International journal of radiation biology*, 1994, **65**, 7-17.
6. W. C. Dewey, C. C. Ling and R. E. Meyn, *International Journal of Radiation Oncology* Biology* Physics*, 1995, **33**, 781-796.
7. J. D. Cox, J. Stetz and T. F. Pajak, *International Journal of Radiation Oncology* Biology* Physics*, 1995, **31**, 1341-1346.
8. G. Cividalli, *Radiation research*, 1963, **20**, 564-576.
9. R. Davey, N. McCoy, M. Yu, J. Sullivan, D. Spiegel and S. Leitman, *Transfusion*, 1992, **32**, 525-528.
10. R. Zimmermann, S. Wintzheimer, V. Weisbach, J. Strobel, J. Zingsem and R. Eckstein, *Transfusion*, 2009, **49**, 75-80.
11. J. A. LaVerne, 2009.
12. W. G. Burns and H. E. Sims, *Journal of the Chemical Society, Faraday Transactions 1: Physical Chemistry in Condensed Phases*, 1981, **77**, 2803-2813.
13. K. Hensley, K. A. Robinson, S. P. Gabbita, S. Salsman and R. A. Floyd, *Free Radical Biology and Medicine*, 2000, **28**, 1456-1462.
14. M. H. Antonelou, A. G. Kriebardis, K. E. Stamoulis, E. Economou‐Petersen, L. H. Margaritis and I. S. Papassideri, *Transfusion*, 2010, **50**, 376-389.
15. E. Niki, Y. Yamamoto, E. Komuro and K. Sato, *The American journal of clinical nutrition*, 1991, **53**, 201S-205S.
16. K. Collard, D. White and A. Copplestone, *Blood Transfusion*, 2014, **12**, 210.
17. G. Moroff and N. Luban, *Transfusion Medicine Reviews*, 1997, **11**, 15-26.
18. H. M. Zbikowska, A. Antosik, M. Szejk, M. Bijak and P. Nowak, *International journal of radiation biology*, 2014, **90**, 1201-1210.
19. A. Khan, K. Manna, D. K. Das, S. B. Kesh, M. Sinha, U. Das, S. Biswas, A. Sengupta, K. Sikder and S. Datta, *Free radical research*, 2015, 1-42.
20. Y. Zhu, J. Li, W. Li, Y. Zhang, X. Yang, N. Chen, Y. Sun, Y. Zhao, C. Fan and Q. Huang, *Theranostics*, 2012, **2**, 302.
21. V. N. Mochalin, O. Shenderova, D. Ho and Y. Gogotsi, *Nat Nano*, 2012, **7**, 11-23.
22. O. A. Williams, J. Hees, C. Dieker, W. Jäger, L. Kirste and C. E. Nebel, *ACS nano*, 2010, **4**, 4824-4830.

23. A. Krueger and D. Lang, *Advanced Functional Materials*, 2012, **22**, 890-906.
24. A. Aleksenskiy, E. Eydelman and A. Y. Vul, *Nanoscience and Nanotechnology Letters*, 2011, **3**, 68-74.
25. W. S. Yeap, S. Chen and K. P. Loh, *Langmuir*, 2008, **25**, 185-191.
26. N. Gibson, O. Shenderova, T. Luo, S. Moseenkov, V. Bondar, A. Puzyr, K. Purtov, Z. Fitzgerald and D. Brenner, *Diamond and Related Materials*, 2009, **18**, 620-626.
27. X. Q. Zhang, R. Lam, X. Xu, E. K. Chow, H. J. Kim and D. Ho, *Advanced materials*, 2011, **23**, 4770-4775.
28. I. I. Kulakova, *Physics of the Solid State*, 2004, **46**, 636-643.
29. V. Vaijayanthimala, Y.-K. Tzeng, H.-C. Chang and C.-L. Li, *Nanotechnology*, 2009, **20**, 425103.
30. K.-K. Liu, C.-L. Cheng, C.-C. Chang and J.-I. Chao, *Nanotechnology*, 2007, **18**, 325102.
31. Y.-C. Lin, L.-W. Tsai, E. Perevedentseva, H.-H. Chang, C.-H. Lin, D.-S. Sun, A. E. Lugovtsov, A. Priezzhev, J. Mona and C.-L. Cheng, *Journal of biomedical optics*, 2012, **17**, 1015121-1015129.
32. J. Li, Y. Zhu, W. Li, X. Zhang, Y. Peng and Q. Huang, *Biomaterials*, 2010, **31**, 8410-8418.
33. M. Harboe, *Scandinavian journal of clinical and laboratory investigation*, 1959, **11**, 66-70.
34. S. O. Sowemimo-Coker, *Transfusion medicine reviews*, 2002, **16**, 46-60.
35. V. V. Danilenko, *Physics of the Solid State*, 2004, **46**, 595-599.
36. J.-B. Donnet, *Carbon black: science and technology*, CRC Press, 1993.
37. B. M. Rothen-Rutishauser, S. Schürch, B. Haenni, N. Kapp and P. Gehr, *Environmental science & technology*, 2006, **40**, 4353-4359.
38. I. Draganic, *The radiation chemistry of water*, Elsevier, 2012.
39. R. Grebe, M. Zuckermann and H. Schmid-Schönbein, in *Electromagnetic Fields and Biomembranes*, Springer, 1988, pp. 141-144.
40. M. Suwalsky, K. Oyarce, M. Avello, F. Villena and C. P. Sotomayor, *Chemico-biological interactions*, 2009, **179**, 413-418.
41. M. Diez-Silva, M. Dao, J. Han, C.-T. Lim and S. Suresh, *MRS bulletin*, 2010, **35**, 382-388.
42. M. Green, C. Noguchi, A. Keidan, S. Marwah and J. Stuart, *Journal of Clinical Investigation*, 1988, **81**, 1669.
43. B. R. Wood and D. McNaughton, *Journal of Raman Spectroscopy*, 2002, **33**, 517-523.
44. I. P. Torres Filho, J. Terner, R. N. Pittman, E. Proffitt and K. R. Ward, *Journal of Applied Physiology*, 2008, **104**, 1809-1817.
45. M. Puchala, Z. Szweda-Lewandowska and J. Kiefer, *Journal of radiation research*, 2004, **45**, 275-279.
46. K. Serrano, D. Chen, A. Hansen, E. Levin, T. Turner, J. Kurach, J. Acker and D. Devine, *Vox sanguinis*, 2014, **106**, 379-381.
47. R. Reverberi, M. Govoni and M. Verenini, *Annali dell'Istituto superiore di sanità*, 2006, **43**, 176-185.
48. A. Bernas and D. Grand, *The Journal of Physical Chemistry*, 1994, **98**, 3440-3443.
49. R. J. Woods and A. K. Pikaev, *Applied radiation chemistry: radiation processing*, John Wiley & Sons, 1994.
50. F. Hutchinson and D. Ross, *Radiation research*, 1959, **10**, 477-489.
51. P. Riley, *International journal of radiation biology*, 1994, **65**, 27-33.
52. M. L. Circu and T. Y. Aw, *Free Radical Biology and Medicine*, 2010, **48**, 749-762.
53. V. Vasilieva, M. Alyakov and M. Apostolova, in *Nanoscience Advances in CBRN Agents Detection, Information and Energy Security*, Springer, 2015, pp. 423-436.
54. R. O. Wright, W. J. Lewander and A. D. Woolf, *Annals of emergency medicine*, 1999, **34**, 646-656.
55. D. M. Close, W. H. Nelson and W. A. Bernhard, *The Journal of Physical Chemistry A*, 2013, **117**, 12608-12615.
56. F. Teyssier, J.-O. Bay, C. Dionet and P. Verrelle, *Bulletin du cancer*, 1999, **86**, 345-357.
57. A. Maity, W. G. McKenna and R. J. Muschel, *Radiotherapy and oncology*, 1994, **31**, 1-13.
58. M. Murphy, T. Wallington, P. Kelsey, F. Boulton, M. Bruce, H. Cohen, J. Duguid, S. Knowles, G. Poole and L. Williamson, *British journal of haematology*, 2001, **113**, 24.
59. L. T. Goodnough, M. E. Brecher, M. H. Kanter and J. P. AuBuchon, *New England Journal of Medicine*, 1999, **340**, 438-447.
60. A. Anand, W. Dzik, A. Imam and S. Sadrzadeh, *Transfusion*, 1997, **37**, 160-165.
61. A. Antosik, K. Czubak, A. Gajek, A. Marczak, R. Glowacki, K. Borowczyk and H. Zbikowska, *Transfusion Medicine and Hemotherapy*, 2015.
62. P. Agarwal, V. Ray, N. Choudhury and R. Chaudhary, *Indian Journal of Medical Research*, 2005, **122**, 385.
63. M. Acosta‐Elías, A. Sarabia‐Sainz, S. Pedroso‐Santana, E. Silva‐Campa, K. Santacruz‐Gomez, A. Angulo‐Molina, B. Castaneda, D. Soto‐Puebla, M. Barboza‐Flores and R. Melendrez, *physica status solidi (a)*, 2015, **212**, 2437-2444.
64. J.-D. Tissot, O. Rubin and G. Canellini, *Current opinion in hematology*, 2010, **17**, 571-577.
65. M. Wortis and R. Mukhopadhyay, *Proceedings of the National Academy of Sciences*, 2002, **99**, 16766-16769.